Materials Horizons

ROYAL SOCIETY OF CHEMISTRY

COMMUNICATION

View Article Online
View Journal | View Issue

Cite this: *Mater. Horiz.*, 2024, 11, 2506

Received 19th November 2023,
Accepted 26th February 2024

DOI: 10.1039/d3mh01959d

rsc.li/materials-horizons

Mechanical metamaterials as broadband electromagnetic wave absorbers: investigating relationships between geometrical parameters and electromagnetic response†

Dahyun Daniel Lim,[a] Sangryun Lee,[ab] Jeong-Ho Lee,[a] Wonjoon Choi *[c] and Grace X. Gu *[a]

The utilization of low-density and robust mechanical metamaterials rises as a promising solution for multifunctional electromagnetic wave absorbers due to their structured porous structures, which facilitates impedance matching and structural absorption. However, the various geometrical parameters involved in constructing these metamaterials affect their electromagnetic response, necessitating a comprehensive understanding of underlying absorbing mechanisms. Through experimentally validated numerical analysis, this study delves into the influence of geometrical factors on the electromagnetic response of representative low-density, high strength mechanical metamaterials, namely octet-truss and octet-foam. By juxtaposing electromagnetic response under varying volume fractions, cell lengths, and multilayer configurations of octet-truss and octet-foam, distinct absorption mechanisms emerge as geometrical parameters evolve. These mechanisms encompass diminished reflection owing to porous structures, effective medium approximations within subwavelength limits, and transmission-driven or reflection-driven phenomena originating from the interplay of open- and closed-cell structures. Through analyses on these mechanical metamaterials, we demonstrate the viability of employing them as tunable yet scalable structures that are lightweight, robust, and broadband electromagnetic wave absorption.

New concepts

This study demonstrates the multifunctional usage of low-density and robust mechanical metamaterials as effective broadband electromagnetic wave absorbers, realizing their impedance matching and structural absorption capabilities originating from their porous lattice structure. The correlation between the geometrical parameters of mechanical metamaterials and the electromagnetic wave response remained unanswered due to the large number of design parameters in the lattice structure and the invisible electromagnetic wave response, making it challenging to define the underlying absorbing mechanisms through an empirical approach. In this work, we elucidate the electromagnetic response and absorbing mechanism of octet-truss and octet-foam, each representing open-strut and closed-shellular mechanical metamaterials, by using experimentally validated numerical analysis. We investigate how geometrical features, including unit cell length, volume fraction, strut/sheet composition, and multilayer structures, affect the transmission, reflection, and absorption of electromagnetic waves in the multi-bandwidth range of 4–18 GHz. This work provides insights into materials science, demonstrating the use of lattice structure as a broadband absorber and enabling the design of application-specific multifunctional metamaterials.

1. Introduction

An electromagnetic wave absorber (EMA) is a functional structure that dissipates incident electromagnetic (EM) wave energy through magnetic or dielectric loss.[1] Increased use of microwave emitting sources in wireless communication and defense applications has gained interest in developing broadband EMAs for mitigating EM radiation exposure or enhancing radar stealth capabilities.[2] Even with recent advances in broadband EM absorbing material such as carbon-based or ferrite-based composites,[3,4] its bulk, heavy, and flat configuration of the raw material with fixed EM properties (permittivity and permeability) limits usage in practical applications that require lightweight, robust and broadband EM wave absorption.[5] To mitigate the limited absorptivity of EM absorbing material with fixed EM properties, structural absorbing methods have been introduced utilizing various three-dimensional designs such as frequency selective surface, laminated structures, or pyramidal structures.[6–10] As EM wave absorption depends on the synergy of the material's EM properties and its geometry, tuning structural parameters of EMAs can offer increased attenuation through optimizing resonance, impedance matching, and increased multiple scattering. However, the three-dimensional EMAs have seldom been utilized in practical

[a] *Department of Mechanical Engineering, University of California, Berkeley, CA 94720, USA. E-mail: ggu@berkeley.edu*
[b] *Division of Mechanical and Biomedical Engineering, Ewha Womans University, Seoul 03760, South Korea*
[c] *School of Mechanical Engineering, Korea University, Seoul 02841, Republic of Korea. E-mail: wojchoi@korea.ac.kr*

† Electronic supplementary information (ESI) available. See DOI: https://doi.org/10.1039/d3mh01959d

applications despite the advantages in broadband absorption. The intrinsic limitations were excessive weight and bulky 3D configuration added to the existing structure, which is not feasible for use in applications like aircraft.

An effective strategy to overcome this challenge involves employing a multifunctional structure, where a porous but structured unit cell design benefits such as low-density, load-bearing, and broadband EMA properties. Such structures are predominantly aimed at broadband EMAs within the microwave spectrum, commonly used in radar systems operating across multiple bands, including C (4–8 GHz), X (8–12 GHz), and Ku (12–18 GHz) bands. For instance, a honeycomb structure fabricated from highly absorbent materials can simultaneously achieve mechanical strength at low-density and broadband EM wave absorption across C, X, and Ku bands, thanks to its engineered porous structure.[11–17] The hexagonal cavities in the honeycomb facilitate EM wave transmission, while the internally angled, shell-like structure intensifies internal attenuation when combined with a coated absorbent material. However, prior work on such multifunctional honeycomb structures has anisotropic absorption depending on the unit cell direction and involved complex manufacturing techniques, including dipping,[11,14] composite impregnation,[12] or vacuum encapsulation[15,16] as detailed in Table S1 (ESI†). A significant advancement in simplifying this process could be the use of 3D printing, a technique already employed for creating efficient EMAs with streamlined fabrication.[5] Examples of 3D printed EMA structures include pyramidal designs,[18–20] gradient absorbers,[21,22] and twisted cross,[23] all demonstrating the combined benefits of EM wave attenuation and structural absorption. Nevertheless, these 3D printed EMAs primarily focus on broadband absorption, often overlooking the aspect of load-bearing in low-density structures.

Recently research has begun to explore the potential of 3D printed structures to achieve multifunctionality. This is achieved by employing lightweight, load-bearing mechanical metamaterials as EMA, such as gyroid,[24] octet-truss,[25] and kelvin-foam[26] structures. Similar to honeycomb design, these structured porous mechanical metamaterials enable enhanced attenuation through structural absorption. They also offer the benefits of simplified production *via* additive manufacturing and isotropic absorption properties. For instance, An *et al.* demonstrated a gyroid-structured 3D printed metasurface capable of achieving a broadband reflection loss (−10 dB) across a 2–40 GHz range.[24] Their study examined the impact of various geometrical parameters, such as volume fraction, strut/sheet configurations in gyroid, and unit cell length, on attenuation performance. The octet-truss, recognized for its low-density and robust mechanical, has also shown significant promise as an effective multifunctional EMA[25] offering improved isotropic mechanical strength and EM wave absorption due to its unique unit cell geometry. Additionally, kelvin-foam, known for its bending-dominated mechanical properties, has proven to be an effective multifunctional EMA, benefiting from its lattice structure.[26] Despite these advancements and experimental validation confirming the potential of proposed mechanical metamaterials as ideal EMAs with streamlined fabrication, the specific EM wave absorbing mechanisms dictated by the unit cell geometry are not fully understood with the limited number of geometrical parameters being explored (Table S1, ESI†). Current research on 3D printed multifunctional EMAs predominantly focuses on demonstrating broadband absorption experimentally, with a limited exploration of geometrical parameters. Unlike mechanical or thermal responses, EM responses (absorption, transmission, and reflection) are not observable, thus limiting the investigation of the absorption mechanism with an empirical approach. Consequently, the relationship between the structural parameters of mechanical metamaterials and their effectiveness in EM wave absorption remains as an uncharted area of study.

The objective of this paper is to methodically explore how the geometrical features of mechanical metamaterials influence EM responses and to identify the fundamental mechanisms of absorption. By examining the relationship between the geometry of these metamaterials and EM wave behavior, specifically in terms of transmission, reflection, and absorption, we aim to enhance the understanding of structural design and optimization beyond merely measuring the reflection loss EMAs. For this comparative study, we have selected two representative low-density, load-bearing structures: octet-truss, and octet-foam. First, we examine the influence of octet-truss and octet-foam's design parameters—cell length, volume fraction, and basic building composition (strut or sheet)—to the EM response. By analyzing these geometrical parameters, absorbing mechanisms are elucidated when specific mechanical metamaterials are used as broadband EMAs. Furthermore, merits of using a multilayered structure as EMAs compared to a single layer structure are explained. Lastly, the effects of oblique incident angles on polarized EM waves on octet-truss and octet-foam are investigated by contrasting the transverse electric and transverse magnetic waves. Exploring geometrical parameters of octet-truss and octet-foam to the EM response and defining the absorbing mechanisms will offer essential design guidelines to create effective multifunctional EMAs.

2. Results and discussion

When considering the configuration of EMAs to fill up a given design space, various strategies to choose the internal geometry are available. One option is to entirely occupy the space with EM wave absorbing material without internal structures, referred to as 'solid material' in this study, as shown in Fig. 1(a). On the other hand, porous structures, such as stochastic sponge structure approximated as an effective medium (Fig. 1(b)) or mechanical metamaterials possessing functional internal architectures (Fig. 1(c) and (d)) can be introduced to enhance impedance matching compared to solid materials. While solid materials exhibit fixed EM properties, mechanical metamaterials offer a range of design parameters that could potentially influence EM response. While there is a plethora of low-density and load-bearing mechanical metamaterials available,[27,28] we select octet-truss and octet-foam in this study

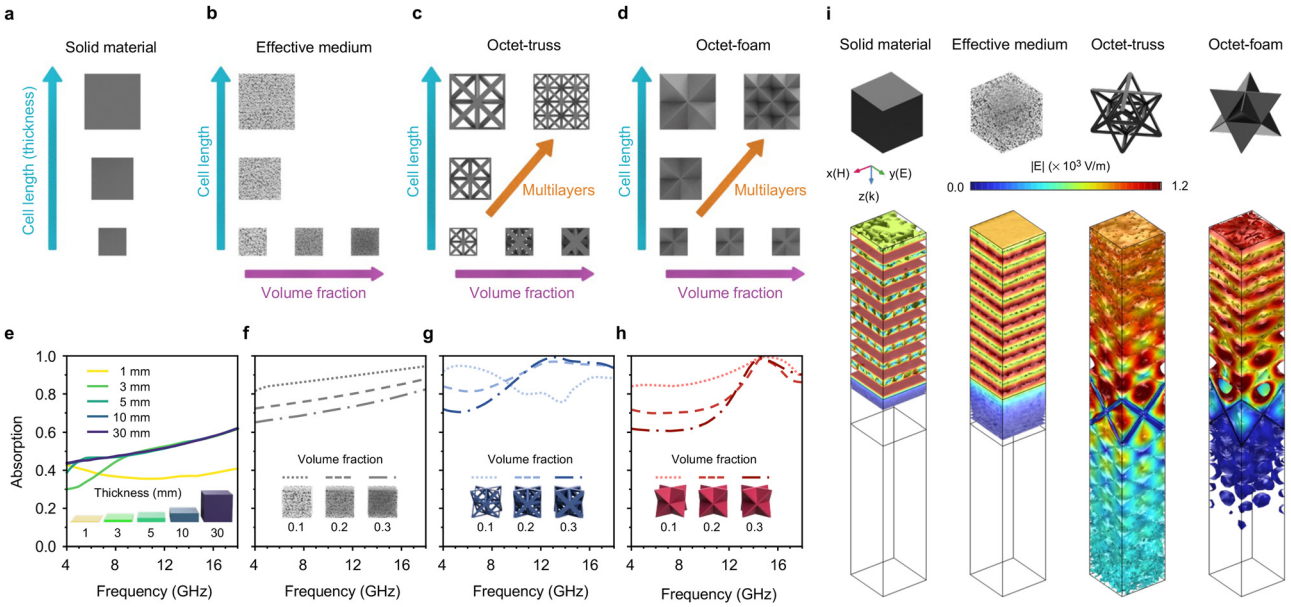

Fig. 1 Comprehensive overview of mechanical metamaterials as a broadband EMA. Depiction of unit cell geometries: (a) solid material, (b) effective medium, (c) octet-truss, and (d) octet-foam. EM wave absorption of these four geometries when exposed to a broadband incident frequency (4–18 GHz): (e) solid material with varying thickness, unit cell structures with 30 mm cell length varying volume fraction of 0.1, 0.2, 0.3: (f) effective medium, (g) octet-truss, and (h) octet-foam. (i) Distribution of electric field on geometries with a 30 mm cell length at incident frequency of 14 GHz.

as these two structures each allows comparison of strut *versus* sheet and open to closed-cell configurations. Numerical analysis is employed to adequately explore the impact of design parameters on EM responses. Here, the material properties of carbon black-based polylactic acid (CB-PLA) are utilized exhibiting high dielectric EM wave attenuation and fabricability as validated with our prior study using 3D printing.[25] The finite element method setup (in the materials and methods section) is validated by comparing numerical results with experimental data, illustrating a reasonable correspondence between the numerical and empirical outcomes (Fig. S1, ESI†). In addition, manufacturability of octet-truss and octet-foam using the CB-PLA material has also been demonstrated in Fig. S1 (ESI†).

2.1. Porous mechanical metamaterial as a broadband EMA

The solid material, an EM absorbing substance with complete absence of porosity (100% infill), demonstrates an absorption limit as thickness increases due to the impedance mismatch between the material and incoming medium (air), as illustrated in Fig. 1(e). By altering the thickness of the solid material within the range of 0.2 mm to 10 mm, convergence in absorption levels is observed as solid material thickens. For instance, thickness surpassing 6 mm regresses into 44.7% at 4 GHz and 62.2% at 18 GHz (Fig. S2, ESI†). As tightly packed solid material limits EM waves to permeate through the structure, thickened material leads to a substantial portion of EM energy being reflected. Thus, the average absorption of the solid material across the 4–18 GHz spectrum is limited to 51.4%. To enhance absorptivity, the introduction of porosity becomes pivotal as it incorporates the presence of air inside the structure, thereby diminishing the impedance mismatch between the dielectric lossy material and the incident medium (air). This facilitates deeper penetration of EM waves into the structure, promoting stronger attenuation through internal scattering and multi-reflections.[29,30]

One approach to introduce porosity to dielectric lossy material is by incorporating a porous, randomized sponge-like structure typically created *via* methods such as freeze drying[31,32] or pyrolysis.[33] Such sponge structures serve as a suitable control group, offering a contrasting randomized internal architecture when compared to mechanical metamaterial. Nevertheless, due to the complexity of modeling intricate randomness of sponge structures, we employ the effective medium approximation as an alternative. This assumes that the porosity within the internal foam structure is relatively small in relation to the incident wavelength's size. Thus, to compare the EM response of the sponge porous foam with solid material, an effective medium model is employed. This model treats the structure's material as a homogenous amalgamation of lossy material (CB-PLA) and air. We use linear approximation of the effective permittivity expressed as eqn (1),[21,34] which is also used in the literature to model homogenization of porous composites.[21,31]

$$\varepsilon_{\text{eff}} = \alpha\varepsilon_{\text{CB-PLA}} + (1 - \alpha)\varepsilon_{\text{air}} \quad (1)$$

Here, ε_{eff} represents the effective permittivity with $\varepsilon_{\text{CB-PLA}}$ and ε_{air} being the permittivity of CB-PLA and air, respectively, while α signifies the volume fraction of CB-PLA. The effective permeability (μ_{eff}) mirrors that of air since CB-PLA manifests with real and imaginary permeability of 1 and 0 (Fig. S1(b), ESI†). Fig. 1(f) shows that by employing an effective medium with reduced CB-PLA's volume fractions 0.3, 0.2, to 0.1, higher EM wave absorption is observed as the proportion of air (porosity) escalates. Across the 4–18 GHz range, the mean

absorption rate is 72.7% for a volume fraction of 0.3, 79.4% for 0.2, and highest absorption of 88.7% for 0.1. The effective medium outperforms the solid material in terms of EM wave absorption over the entire C, X, and Ku bandwidths. It is important to underscore, however, that the effective medium is a theoretical construct representing a composite of CB-PLA and air that raises design and fabrication challenges. A structure closely resembling this concept is a porous foam structure with random porosity, yet it may lack mechanical robustness and exhibit difficulties in precisely controlling the volume fraction of the CB-PLA composite.[29,30,35,36] Consequently, the utilization of mechanical metamaterials possessing internal architectures to control porosity, octet-truss or octet-foam, could potentially offer viable alternatives to the porous foam. These structures could enable broadband EM wave absorption *via* adjustments in the geometrical parameters while ensuring manufacturability through 3D printing.

To validate this, we investigate octet-truss and octet-foam structures, maintaining a constant cell length of 30 mm while reducing the volume fraction from 0.3 to 0.1 illustrated in Fig. 1(g) and (h). The outcomes demonstrate that both octet-truss and octet-foam surpass the absorption capabilities of the solid material with an identical cell length across the entire 4–18 GHz spectrum with frequency spacing of 0.5 GHz. While the effective medium manifests a gradual change in absorption levels due to consistent structure, octet-truss, and octet-foam display unique fluctuations with prominent peaks at specific frequencies. For instance, octet-truss exhibits a peak absorption at 5 GHz for a volume fraction of 0.1 and at 14 GHz for volume fractions of 0.2 and 0.3, as shown in Fig. 1(g).

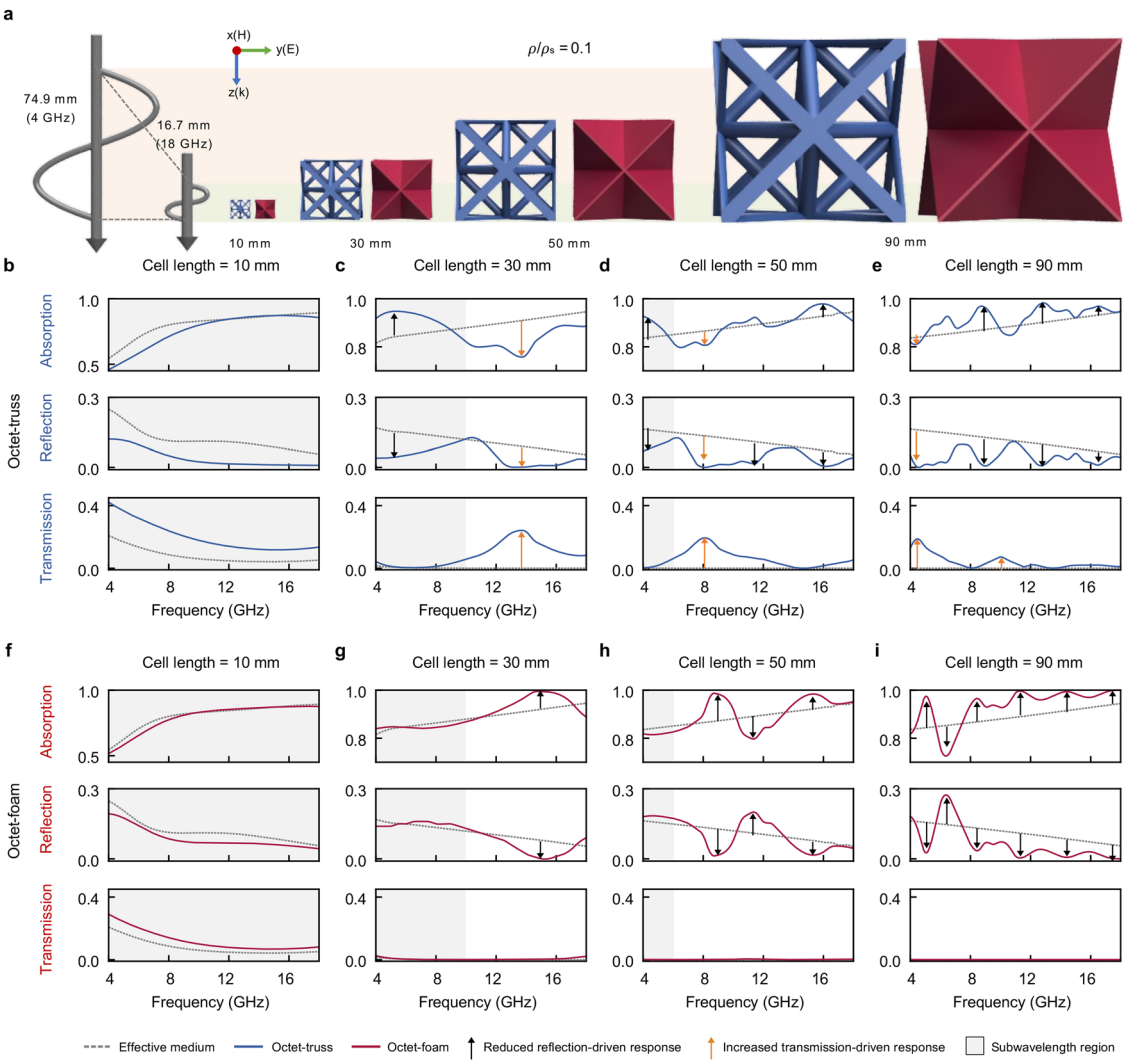

Fig. 2 Correlation between EM response and the mechanical metamaterials' cell length. (a) Diagram illustrating the scale of incident wavelengths, ranging from 74.9 mm (at 4 GHz) to 16.7 mm (at 18 GHz), in comparison to octet-truss and octet-foam with cell length of 10 mm, 30 mm, 50 mm, and 90 mm. (b)–(e) EM response curves for octet-truss with cell length (b)10 mm, (c) 30 mm, (d) 50 mm, (e) 90 mm, and for octet-foam with cell length (f)10 mm, (g) 30 mm, (h) 50 mm, (i) 90 mm. The effective medium's response is depicted in grey dashed line for comparison, while the light grey background signifies incident wave range longer than the cell length. Orange and black arrows each indicate increased transmission-driven and reduced reflection-driven responses.

Conversely, octet-foam exhibits a notable peak absorption around 15.5 GHz across all volume fractions (Fig. 1(h)). These initial findings underscore that the geometry of mechanical metamaterials holds a considerable influence over the EM response. In addition, a comparison of the 3D electric field distribution at 14 GHz in Fig. 1(i), encompassing the solid material, effective medium, octet-truss, and octet-foam, highlights the marked disparities in how the incident wave interacts with the structure. The electric field only forms outside the surface of the solid material, and the electric field on the effective medium gradually diminishes throughout the structure without transmission. In contrast, both octet-truss and octet-foam illustrate internal transmission of the incident wave, engendering internal multi-reflections and scattering that amplify the attenuation.

2.2. Influence of geometrical parameters of mechanical metamaterials to the EM response

To comprehensively understand the EM response of octet-truss and octet-foam, a thorough exploration of their geometrical parameters, including cell length and constituent subcomponents (strut and sheet), becomes crucial. Hence, we analyze the absorption, transmission, and reflection of EM waves across a spectrum of four distinct cell lengths (10 mm, 30 mm, 50 mm, and 90 mm) with 0.1 volume fraction for both octet-truss and octet-foam under the broadband incident wave ranging from 74.9 mm (at 4 GHz) to 16.7 mm (18 GHz) as illustrated in Fig. 2(a). The chosen cell lengths effectively encapsulate scenarios where the cell length is either smaller (10 mm), partially smaller (30 mm and 50 mm), or larger (90 mm) than the broadband range of incident wavelength (16.7–74.9 mm).

At a cell length of 10 mm, smaller than the entire span of incident wavelengths (16.7–74.9 mm), both octet-truss (Fig. 2b) and octet-foam (Fig. 2f) demonstrate a closely aligned EM response behavior with the effective medium, represented by the gray dashed line. The correlation coefficients between the effective medium and octet-truss, as well as octet-foam, stand at 0.97 and 0.99, respectively. This strong correlation can be elucidated by the effective medium theory, which assumes that geometry can be approximated as an effective medium when its constituent elements are notably smaller than the incident wavelength. While the 10 mm cell length is not significantly smaller than the incident wavelength range, the subcomponents forming the octet-truss (struts) or octet-foam (sheets) are sufficiently minimal. For instance, a 10 mm cell length with a volume fraction of 0.1, the strut diameter of the octet-truss measures 0.93 mm, and the sheet thickness of the octet-foam is 0.15 mm.

While a 10 mm cell length octet-truss or octet-foam shows ineffective EM wave absorption below 90% across the 4–18 GHz range, absence of a perfect electric conductor (PEC) on the base should be noted. Introducing a PEC at the base holds the potential to significantly amplify absorption by nullifying transmission and elevating internal dissipation through reflection upon reaching the base, which is commonly used in the design of EMAs. This adjustment of putting PEC on the bottom can easily result in an average absorption surpassing 90% across broadband frequencies for both octet-truss and octet-foam (Fig. S3, ESI†). However, in the context of this study, we deliberately excluded the use of a PEC to enable a clear observation of the differing transmission behaviors among the various structures.

As the cell length of octet-truss and octet-foam surpass the incident wavelength (30 mm, 50 mm, and 90 mm), the EM response begins to be affected by the geometry, revealing structural absorption alongside inherent material properties as shown in Fig. 2(c)–(e) and (g)–(i). In these scenarios, multiple local maxima (peaks) and local minima (valleys) emerge in absorption, transmission, and reflection, which marks a discernible contrast to cases with smaller cell lengths (10 mm). As the overall dimensions of octet-truss and octet-foam enlarge relative to the incident wavelength, the dimensions of their constituent elements—struts and sheets—also increase in diameter, length, and thickness. Consequently, not all the incident waves are absorbed; instead, partially transmitted and reflected EM waves induce multiple internal reflections and scattering, leading to the superposition of the EM wave interferences within the structure. The resulting superposition generates destructive or constructive interference contingent on the wavelength that results in peaks and valleys in absorption. For example, at 15 GHz in Fig. S4 (ESI†), the power loss density plot for both octet-truss and octet-foam displays a gradient dissipation across the structure in 10 mm cell length, while several concentrated loss regions observed throughout the structure for a 30 mm geometry.

The EM response of the octet-truss demonstrates distinct absorbing characteristics, including increased transmission-driven and reduced reflection-driven responses, as depicted by the orange and black arrows in Fig. 2(c)–(e). The open-cell configuration of the octet-truss enables EM waves to traverse through the struts, leading to multiple internal reflections occurring among struts positioned at various angles, thereby engendering constructive and destructive interferences as shown with power loss density plot in Fig. S6 (ESI†). The interference-based absorption stemming from EM wave transmission within the structure can have dual implications for the design of EMAs. While it generally enhances absorption by allowing EM wave to transmit further within the structure, the transmission-driven response could establish pathways that create constructive interference at the structure's base at specific frequencies, resulting in peak transmissions that detract from absorption. For instance, in the case of a 50 mm octet-truss, the absorption oscillates between increased transmission at 8 GHz and reduced reflection response at 16 GHz, as depicted in Fig. 2(d). When internally reflected waves lead to constructive interference at the base of the octet-truss, transmission increases, as observed in the electric field plot at 8 GHz (Fig. 3(a)). Conversely, interference causing reduced reflection and diminished transmission yields peak absorption at 16 GHz (Fig. 3(b)). In the range between these absorption peaks and valleys, concentrated power loss regions shift across different positions of the struts within the octet-truss, inducing fluctuations in the EM response (Fig. S6, ESI†). The count of

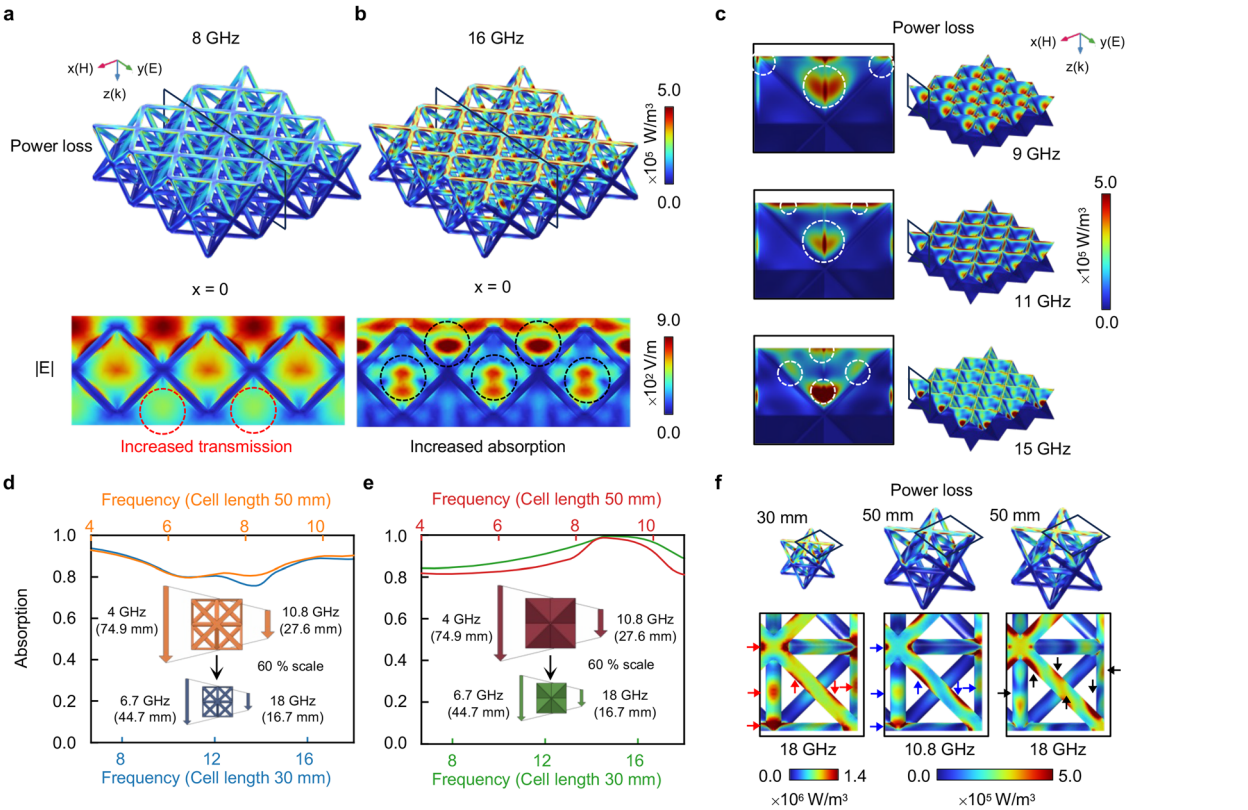

Fig. 3 EM wave absorbing mechanisms of octet-truss and octet-foam. Power loss density and electric field plot on a 50 mm octet-truss structure at (a) 8 GHz and (b) 16 GHz. (c) Power loss density plot across a 50 mm octet-foam at 9 GHz (top), 11 GHz (middle), and 15 GHz (bottom). (d) and (e) Exploring EM wave absorption in correlation to the relative cell length of octet-truss and octet-foam. (f) A comparative assessment of power loss density plot of octet-truss under equal relative cell length conditions against equal incident wavelength conditions.

transmission and reflection peaks and valleys grows with the increase in cell length due to the increased relative length of the octet-truss compared to the incident wavelength, generating more locations for interferences.

In contrast, octet-foam manifests stronger resonances in absorption originating from the reflection-based response due to its sheet-based composition (Fig. 2(g)–(i)). This stems from the closed-cell structure of the octet-foam, which restricts EM wave transmission through the geometry compared to the open-cell geometry (octet-truss). Another notable absorbing mechanism of octet-foam involves periodic absorption fluctuations due to the constructive and destructive interferences with reflected waves. For instance, in the power loss density plot at a 50 mm octet-foam (Fig. 3(c)), the locations of power loss concentration (indicated by white dashed line) gradually shift with increased incident frequency. At 9 GHz (first absorption peak), power loss is concentrated at the tips of top cross-section and edges created by angled sheets. Conversely, at 11 GHz, the concentration shifts to the upper edges (forming an X shape) with relatively diminished concentration at the angled sheets. However, as the relative length of the sheet increases with decreased wavelength, the number of concentrations increases, leading to the emergence of a second absorption peak at 15 GHz.

Besides differences in EM wave absorbing mechanism of octet-foam and octet-truss, a common mechanism is that EM response is highly correlated even with varying cell length as long as the relative cell length (the ratio of cell length to the incident wavelength) remains constant. For example, the EM wave absorption of 30 mm and 50 mm cell lengths exhibit a strong correlation when the structures maintain an equal relative cell length, as depicted in Fig. 3(d) and (e). Additionally, the power loss density plots demonstrate marked similarities in the locations of power loss concentration under the same relative cell length, as compared to those with the identical absolute incident wavelength (Fig. 3(f)). At the same relative cell length, the position of the power loss concentration at 18 GHz for the 30 mm cell length (highlighted by red arrows) closely aligns with the position at 10.8 GHz for the 50 mm cell length (indicated by blue arrows). This proximity in peak positions contrasts when the same incident wavelength of 18 GHz is applied to the 50 mm cell length (denoted by black arrows).

In practical scenarios, centimeter-scale structures such as octet-truss or octet-foam structures could serve as stealth enclosures in structural applications, effectively concealing highly reflective objects from monostatic radar detection. Fig. S5 (ESI†) presents an example where a component made from a perfect electric conductor (such as metal parts) is easily detectable by a 14 GHz monostatic radar due to its reflectivity (reflection loss of −2.5 dB). Conversely, employing a 30 mm unit cell length of either octet-truss or octet-foam can significantly diminish the

reflected electromagnetic waves, achieving −14.5 dB and −10.39 dB in reflection loss, respectively, thus demonstrating their efficacy as EMA structures. In contrast, when using a CB/PLA plate of the same mass as the 30 mm octet-truss or octet-foam (with a thickness of 3 mm), only a marginal decrease in reflection (−3.55 dB) is observed. This minimal reduction can be attributed to the lack of structural interaction required for enhanced absorption.

In contrast to octet-truss and octet-foam, which exhibit peak absorption approaching near-perfect absorbance at specific frequencies, the effective medium represented by the grey dashed line in Fig. 2(b)–(i), remains relatively constant regardless of the increase in cell length (30 mm, 50 mm, and 90 mm). This is attributed to the fact that the effective medium is structurally uniform, lacking in structural absorption effects seen in octet-truss or octet-foam. Thus, leveraging the structural

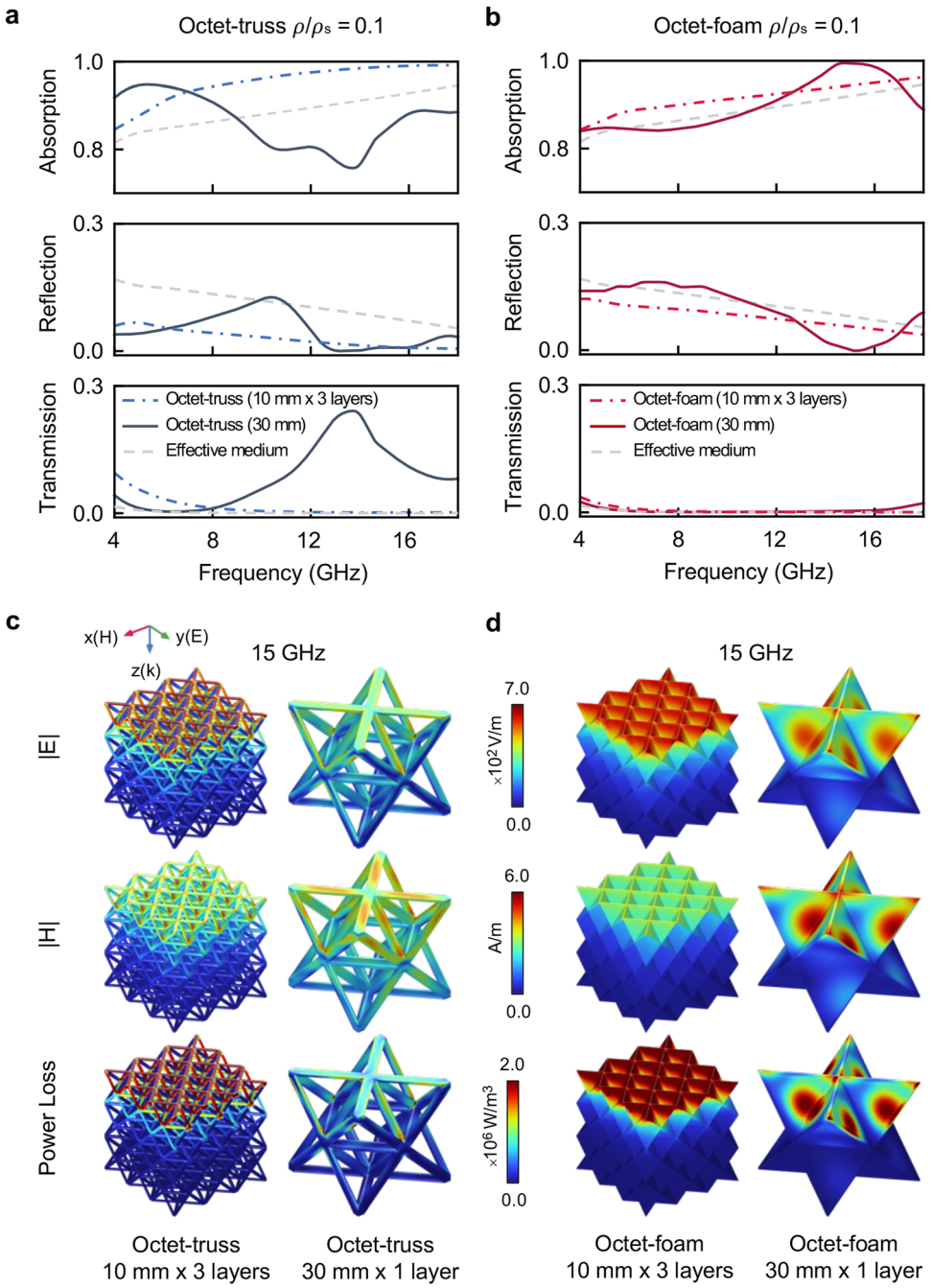

Fig. 4 Analysis of EM response in multilayer structures. Examination of electromagnetic wave absorption, reflection, and transmission in a multilayer arrangement for (a) octet-truss and (b) octet-foam under 30 mm thickness. 3D plots illustrating electric field, magnetic field, and power loss density plot in (c) octet-truss and (d) octet-foam, comparing the multilayer configuration, consisting of three layers with 10 mm cell length each, to the single-layer setup with 30 mm cell length at 15 GHz.

absorption effect of octet-truss or octet-foam, involving multiple internal reflections, scattering, and resonant absorption, could potentially yield higher absorption than a homogenized medium under the same volume fraction in specific frequency ranges based on the application's requirement.

2.3. EM response of a multilayered mechanical metamaterial

The mechanical metamaterials like octet-foam and octet-truss encompass periodicity, enabling the manipulation of repeating unit cell numbers under the same thickness. For instance, octet-truss with a 30 mm cell length can be matched with stacking three layers of octet-truss with 10 mm cell length with equal volume fraction. But this multilayer structure differently affects the EM responses in octet-truss and octet-foam. When the volume fraction is fixed at 10% and the total thickness is set to 30 mm, the multilayered structure notably enhances the absorption especially in octet-truss (Fig. 4(a) and (b)). This increased absorption of multilayered octet-truss arises because of open-cell geometry manifests higher transmission with 10 mm. By arranging the highly transmissive 10 mm octet-truss in a multilayer layout, the EM wave that traverses the first layer is sequentially absorbed across subsequent layers, resulting in broadband absorption spanning 4–18 GHz. Notably, this multilayered octet-truss configuration exhibits a substantial average absorption of 97.6% within the X (8–12 GHz), and Ku (12–18 GHz) bands, which also closely aligns with experimental findings for multilayer structures in prior research (Fig. S1(d), ESI†).[25]

While the bandwidth for attenuation exceeding 90% in a multilayered octet-truss structure (comprising three 10 mm layers) is broader than that of a single 30 mm layer, as shown in Fig. 4 (a), single-layered octet-truss with a larger unit cell size can still be advantageous for specific applications, such as a pass band filter.[37] In scenarios like frequency-selective radome, a distinctive type of absorber is necessary. Here, the radome – a protective cover for radar – must permit certain frequencies to pass through (thus transmitting signal from internal antenna) while absorbing broadband frequencies outside this specified range. Frequency-selective surfaces are commonly employed for such purposes.[37–39] An octet-truss structure with high transmission at specific frequencies, like a peak transmission of 24.0% at 13.5 GHz for a 30 mm octet-truss, could effectively function as a band-pass filter. Additionally, this approach offers mechanical advantages to the radome structure, such as enhanced robustness while maintaining a lightweight profile.

On the other hand, if octet-foam is formed in a multilayer configuration, it exhibits similar absorption, reflection, and transmission to the effective medium across the entire 4–18 GHz range without major increment in the absorption compared to the single layered 30 mm cell length structure. This phenomenon occurs because the closed-cell structure of the octet-foam, even with a 10 mm cell length, restricts transmission, leading to comparatively lower absorption in the subsequent layers as opposed to open-cell structure of octet-truss. Moreover, the multilayered octet-foam structure loses the benefit of strong resonant absorption found in larger cell length (30 mm), due to the reduced impact of its smaller subcomponents. Another advantage of employing larger cell length in octet-foam, in addition to resonant absorption, lies in manufacturability. For instance, with a 10% volume fraction, the sheet thickness of octet-foam is 0.15 mm for a 10 mm cell length, whereas it increases to 0.45 mm for a 30 mm cell length. Considering fused filament fabrication (FFF) as the assumed fabrication method for this study (Fig. S1, ESI†), a 0.45 mm sheet thickness can be manufactured using a standard 0.4 mm nozzle commonly found in FFF 3D printers. Therefore, larger cell length octet-foam not only offers resonant absorption but also facilitates easier fabrication compared to structures with multilayered smaller cell length.

To highlight the differences in EM absorbing mechanisms within multilayered octet-truss and octet-foam, power loss density, electric field, and magnetic field plots are compared (Fig. 4(c) and (d)). At 15 GHz, these four configurations (comprising three-layer and single-layer octet-truss, as well as three-layer, and single-layer octet-foam) exemplify discernible patterns of EM wave absorptions. Overall, across the electric field, magnetic field, and power loss plots, both multilayer structures of octet-truss and octet-foam exhibit a gradient absorption of EM waves. For three-layer octet-truss, while most of the absorption transpires within the first layer, with the presence of the second and third layers, subsequent absorption occurs in the regions where the transmitted waves from the previous layer. A side view, as depicted in Fig. S7 (ESI†), also reveals that octet-truss exhibits heightened absorption in the uppermost first and second layers in the power loss plot. In contrast, three-layer octet-foam displays limited absorption mainly within the initial layer due to its low transmission properties. However, for cell length of 30 mm, interferences from multiple internal reflections yield results in peak and valley in absorption. Hence, the impact of multilayer structures on EM response varies based on the underlying metamaterial structures.

2.4. Influence of incident angle and polarization on the EM response of mechanical metamaterials

To investigate the variations in EM response of octet-foam and octet-truss with incident angle, we conduct a comparative analysis. This analysis involved the study of a 30 mm octet-truss and octet-foam, both with a 10% volume fraction, under transverse electric (TE) and transverse magnetic (TM) polarizations. The incident angles ranged from 0° to 75°, with increments of 15°, as demonstrated in Fig. 5. Given that both octet-truss and octet-foam have geometries symmetrically rotational by 90°, they exhibit polarization insensitivity at a 0° incident angle, indicated by red line in Fig. 5(a)–(d). However, as the incident angle increases, disparities in absorption start to emerge between TE and TM polarizations. This variance is attributed to the changing angle between the electric field's oscillation direction and the dielectric lossy material-based geometry, which differs for TE and TM polarization with increasing incident angles. For octet-foam under TE polarization as in Fig. 5(a), absorption remains relatively unchanged up

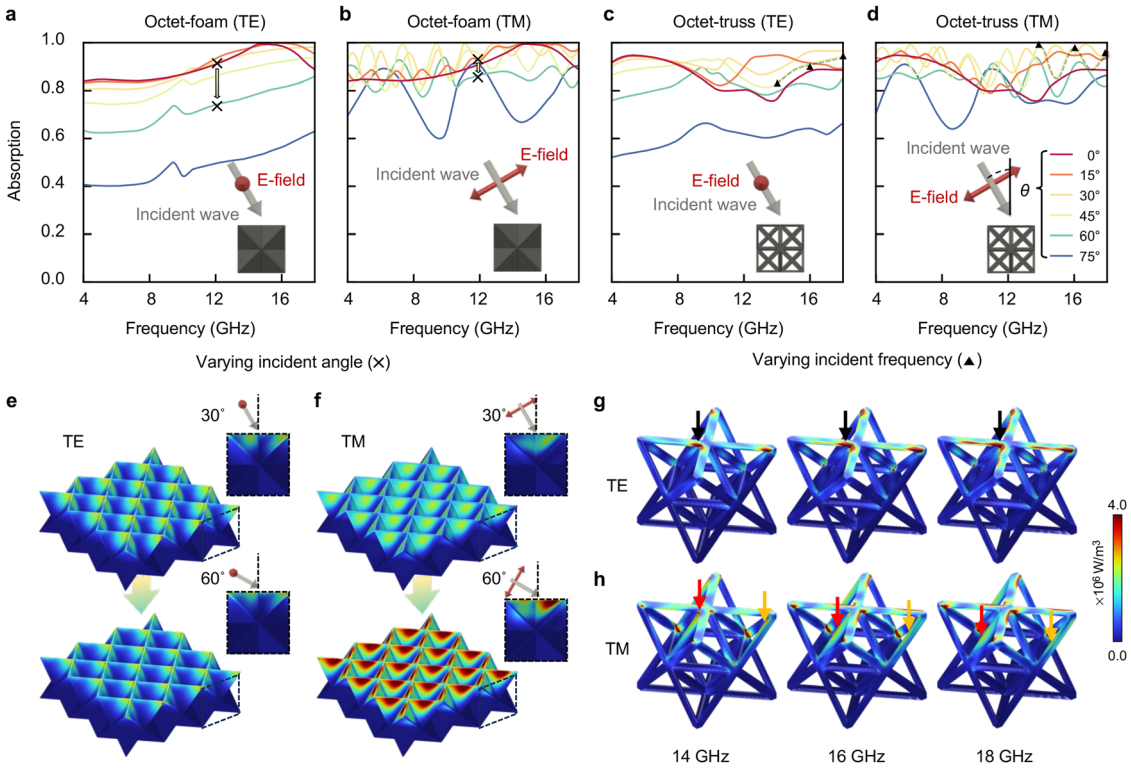

Fig. 5 Comparative examination of electromagnetic wave absorption in octet-truss and octet-foam with varied incident wave angles and polarization. Depicting the EM wave absorptions of (a) and (b) octet-foam and (c) and (d) octet-truss with respect to transverse electric (TE) and transverse magnetic (TM) polarizations. Analyzing the power loss density plot of octet-foam at incident angles of 30° and 60° for (e) TE and (f) TM polarization and octet-truss at 14 GHz, 16 GHz, and 18 GHz under a 45° incident angle for both (g) TE and (h) TM polarizations.

to a 30° incident angle, but then sharply decreases with further increase in angle. On the other hand, for octet-foam under TM polarization, there is a consistently high average absorption level exceeding 86.0% across the 4–18 GHz, which is sustained up to a 60° incident angle (Fig. 5(b)).

The power loss density plot further elucidates this difference in absorbing response of octet-foam between TE and TM polarization. At 12 GHz, for instance, a distinct power loss concentration pattern emerges when we compare incident EM waves of 30° and 60° that are marked with '×' in Fig. 5(a) and (b). Here, the absorption for TE polarization decreases from 91.8% at 30° to 74.2% at 60°, whereas for TM polarization, it changes from 93.1% at 30° to 86.5% at 60°. In the case of TE polarization (Fig. 5(e)), the power loss is primarily localized along the X-shaped upper edge of the octet-foam at both 30° and 60° incident angles. The density of this concentration decreases as the angle increases, corresponding to consistent direction of the electric field. On the other hand, for TM polarization (Fig. 5(f)), changes in the electric field oscillation direction lead to varying positions of power loss concentration. However, the concentration remains significant, as shown in the side view of the octet-foam under TM polarization in Fig. 5(f). Fig. S8 (ESI†) further details the changes in power loss concentration in octet-foam across a range of incidents from 0° to 75°, aligning with the observed variances.

In comparison, octet-truss exhibits a different behavior than octet-foam, which allows angled electric fields to permeate its interior due to its open-cell design, resulting in consistent mean absorption of over 80% up to an incident angle of 60° for both TE and TM polarization. In TE polarization, it is worth noting that while octet-foam experiences gradual decline in absorption as the incident angle increases, octet-truss maintains or even enhances absorption through diagonally arranged struts, which facilitates internal scattering and multiple reflections. The power loss concentration in the octet-truss is more evenly distributed throughout its structure under both TE and TM conditions, as evidenced in Fig. S8 (ESI†). A key difference between octet-truss to octet-foam is observed in their response to increasing incident angles under TE polarization. In the case of octet-truss, absorption rates rise with the angle increase, for example, from 80.5% at 0° to 89.9% at 15°, and 90.0% at 30°. Fig. S8's (ESI†) power loss density comparisons under these conditions reveal that the loss concentration in the octet-truss is dispersed throughout the structure, even reaching to bottom of the structure in TE polarization (at 15°). This dispersion results from the internally scattered EM waves interacting with the octet-truss's rounded struts, leading to increased power loss concentration in different spots at higher angles. In contrast, the octet-foam, with its sheet-based composition, primarily exhibits directional reflection, resulting in diminished attenuation as the incident angle increases.

Finally, a shared characteristic between octet-foam and octet-truss within angled incident EM wave is the frequency-dependent absorption response. In the case of TE polarization,

absorption varies smoothly with changes in incident frequency for both octet-foam (Fig. 5(a)), and octet-truss (Fig. 5(c)). On the other hand, for TM polarization, there are resonance-like fluctuations in absorption intensity as the frequency shifts (octet-foam for Fig. 5(b), and octet-truss for Fig. 5(d)). This distinct behavior is attributed to TE polarization's electric field propagating perpendicular to the structure, leading to minimal alterations in the locations of power loss concentrations as the wavelength changes. On the other hand, TM polarization's electric field orientation shifts in the positions of power loss concentration throughout the structure with alterations in incident wavelength. For instance, when the incident frequency changes from 14 to 18 GHz under a 45° incident angle for both TE and TM polarization in octet-truss (marked as '▲' in Fig. 5(c), and (d)), the power loss concentration positions remain relatively unchanged in TE polarization (marked with black arrows in Fig. 5(g)), while the positions undergo significant displacement under TM polarization (marked with red and orange arrows in Fig. 5(h)).

3. Conclusion

In this paper, we have established a linkage between the geometrical parameters to electromagnetic responses for both the octet-truss and octet-foam and provided design guidance to engineer multifunctional EMAs. Especially, octet-truss and octet-foam are known for their mechanical strength at low densities. The establishment of various absorption mechanisms that can be achieved by fine-tuning parameters like cell type (open and closed), the nature of constituent subcomponents (struts and sheets), volume fraction, cell length, and multilayer configurations was accomplished through a series of detailed numerical analyses. The insights regarding the diverse attenuation mechanisms influenced by geometrical parameters will serve as a fundamental guideline in applying unit cell structures to diverse mechanical, thermal, or acoustic applications and further to multifunctional unit cell structures in EMAs. Our findings lead to a customized EMA design approach suggesting the importance of adjusting metamaterial geometry to meet specific application requirements.

4. Materials and methods

Unit cell geometries definition and material characterization

The COMSOL Multiphysics software's 3D modeling tool is employed to model octet-truss, octet-foam, effective medium, and solid material. Both the octet-truss and octet-foam structures are modeled based on a face-centered cubic octet configuration. The octet-truss is constructed by linking the vertices of an octahedron using struts of equal size. On the other hand, the octet-foam is designed by combining shellular tetrahedral prisms with sheet with identical thickness. To manipulate the volume fraction of the octet-truss and octet-foam, adjustments are made to the diameter of the struts in the case of octet-truss and the thickness of the sheets for octet-foam. For both the effective medium and solid material configurations, volume fraction is controlled for a varying material of the boxed structure, incorporating the effective property eqn (1), wherein the measured relative permittivity (ε) and relative permeability (μ) values of carbon black-polylactic acid (CB-PLA) within the range of 8.2–12.4 GHz are employed (Fig. S1, ESI†). The manufacturability of the designed octet-truss and octet-foam structure is tested using a 3D printer (Ultimaker S3), which utilizes CB-PLA material (Conductive filament, Protopasta) (Fig. S1, ESI†).

Electromagnetic wave simulations

For our simulations, we investigate the electromagnetic responses of the structures, focusing on transmission, absorption, and reflection. To achieve this, we employ the COMSOL Multiphysics RF module. Mechanical metamaterials are represented as a 3D array, with Floquet-periodic boundary conditions applied to all four sides, as depicted in Fig. S1 (ESI†). The material for the geometry is CB-PLA, while the remaining space is filled with air. In the simulation setup, two ports are positioned to assess scattering parameters, specifically the reflection (S_{11}) and transmission (S_{21}) coefficients. The incident electromagnetic waves span within the C, X, and Ku bands (4–18 GHz), and domains outside the ports are designated as perfectly matched layers (PMLs) to minimize unwanted reflections. We utilize tetrahedral mesh generation with physics-controlled settings from COMSOL. This approach ensures that the maximum size of the element is smaller than 4.2% of the incident wavelength. For instance, when creating mesh for a 30 mm octet-truss subjected to 18 GHz incident wave, this method results in around 149 000 domain elements. From the derived scattering parameters, reflection (R) and transmission (T) are calculated using $R = |S_{11}|^2$ and $T = |S_{21}|^2$. The absorption (A) value is then calculated through the equation $A = 1 - R - T$.

Author contributions

All authors contributed to the design and implementation of the research, analysis of the results, and writing of the manuscript.

Conflicts of interest

There are no conflicts of interest to declare.

Acknowledgements

This research was supported by the Prytanean Foundation, Alfred P. Sloan Foundation, the National Science Foundation Extreme Science and Engineering Discovery Environment (XSEDE) Bridges system (Fund number: ACI-1548562), and the University of California, Berkeley Molecular Graphics and Computation Facility (Fund number: NIH S10OD034382).

References

1 X. Zeng, X. Cheng, R. Yu and G. D. Stucky, *Carbon*, 2020, **168**, 606–623.
2 M. I. Hussein, S. S. Jehangir, I. Rajmohan, Y. Haik, T. Abdulrehman, Q. Clément and N. Vukadinovic, *Sci. Rep.*, 2020, **10**, 1–11.
3 F. Qin and C. Brosseau, *J. Appl. Phys.*, 2012, **111**, 4.
4 V. B. Bregar, *IEEE Trans. Magn.*, 2004, **40**, 1679–1684.
5 D. Yang, H. Mei, L. Yao, W. Yang, Y. Yao, L. Cheng, L. Zhang and K. G. Dassios, *J. Mater. Chem. C*, 2021, **9**, 12010–12036.
6 R. S. Anwar, L. Mao and H. Ning, *Appl. Sci.*, 2018, **8**, 1689.
7 Y. Danlée, I. Huynen and C. Bailly, *Appl. Phys. Lett.*, 2012, **100**, 213105.
8 M.-J. Park, J. Choi and S.-S. Kim, *IEEE Trans. Magn.*, 2000, **36**, 3272–3274.
9 W. Li, T. Wu, W. Wang, P. Zhai and J. Guan, *J. Appl. Phys.*, 2014, **116**, 044110.
10 C. Jayalakshmi, A. Inamdar, A. Anand and B. Kandasubramanian, *J. Appl. Polym. Sci.*, 2019, **136**, 47241.
11 H. Pang, Y. Duan, X. Dai, L. Huang, X. Yang, T. Zhang and X. Liu, *J. Mater. Sci. Technol.*, 2021, **88**, 203–214.
12 B.-S. Kwak, G.-W. Jeong, W.-H. Choi and Y.-W. Nam, *Compos. Struct.*, 2021, **256**, 113148.
13 H. Wang, X. Xiu, Y. Wang, Q. Xue, W. Ju, W. Che, S. Liao, H. Jiang, M. Tang and J. Long, *Composites, Part B*, 2020, **202**, 108378.
14 S. Xie, Z. Ji, Y. Yang, G. Hou and J. Wang, *J. Build. Eng.*, 2016, **7**, 217–223.
15 H. Luo, F. Chen, X. Wang, W. Dai, Y. Xiong, J. Yang and R. Gong, *Composites, Part A*, 2019, **119**, 1–7.
16 W.-H. Choi and C.-G. Kim, *Composites, Part B*, 2015, **83**, 14–20.
17 W. Jiang, L. Yan, H. Ma, Y. Fan, J. Wang, M. Feng and S. Qu, *Sci. Rep.*, 2018, **8**, 4817.
18 X. Lleshi, T. Q. Van Hoang, B. Loiseaux and D. Lippens, *IEEE Antennas Wireless Propag. Lett.*, 2020, **20**, 28–32.
19 X. Chen, Z. Wu, Z. Zhang and Y. Zou, *Opt. Laser Technol.*, 2020, **124**, 105972.
20 W.-L. Song, Z. Zhou, L.-C. Wang, X.-D. Cheng, M. Chen, R. He, H. Chen, Y. Yang and D. Fang, *ACS Appl. Mater. Interfaces*, 2017, **9**, 43179–43187.
21 L. Yin, J. Doyhamboure, X. Tian and D. Li, *Composites, Part B*, 2018, **132**, 178–187.
22 L. Yin, X. Tian, Z. Shang and D. Li, *Mater. Lett.*, 2019, **239**, 132–135.
23 H. Mei, W. Yang, X. Zhao, L. Yao, Y. Yao, C. Chen and L. Cheng, *Mater. Des.*, 2021, **197**, 109271.
24 Q. An, D. Li, W. Liao, T. Liu, D. Joralmon, X. Li and J. Zhao, *Adv. Mater.*, 2023, 2300659.
25 D. D. Lim, J. Park, J. Lee, D. Noh, J. Lee, J. Choi and W. Choi, *Addit. Manuf.*, 2022, **55**, 102856.
26 J. Lee, D. D. Lim, J. Park, J. Lee, D. Noh, G. X. Gu and W. Choi, *Small*, 2023, 2305005.
27 J. Berger, H. Wadley and R. McMeeking, *Nature*, 2017, **543**, 533–537.
28 X. Yu, J. Zhou, H. Liang, Z. Jiang and L. Wu, *Prog. Mater. Sci.*, 2018, **94**, 114–173.
29 D. Wang, J. Jin, Y. Guo, H. Liu, Z. Guo, C. Liu and C. Shen, *Carbon*, 2023, **202**, 464–474.
30 D. Wang, M. Zhang, Y. Guo, T. Bai, H. Liu, C. Liu and C. Shen, *J. Mater. Chem. C*, 2022, **10**, 5311–5320.
31 X. Sun, Y. Li, Y. Huang, Y. Cheng, S. Wang and W. Yin, *Adv. Funct. Mater.*, 2022, **32**, 2107508.
32 W. Liu, H. Li, Q. Zeng, H. Duan, Y. Guo, X. Liu, C. Sun and H. Liu, *J. Mater. Chem. A*, 2015, **3**, 3739–3747.
33 L. Liu, S. Yang, H. Hu, T. Zhang, Y. Yuan, Y. Li and X. He, *ACS Sustainable Chem. Eng.*, 2018, **7**, 1228–1238.
34 A. Sihvola, *Subsurface sensing technologies and applications*, 2000, **1**, 393–415.
35 W. Ma, X. Liu, Z. Qiu, Z. Cai, J. Diao and Y. Huang, *Carbon*, 2022, **196**, 913–922.
36 X. Zheng, H. Lee, T. H. Weisgraber, M. Shusteff, J. DeOtte, E. B. Duoss, J. D. Kuntz, M. M. Biener, Q. Ge and J. A. Jackson, *Science*, 2014, **344**, 1373–1377.
37 F. Costa and A. Monorchio, *IEEE Trans. Antennas Propag.*, 2012, **60**, 2740–2747.
38 T.-K. Wu, *Encyclopedia RF Microwave Engineering*, 1995.
39 A. Abbaspour-Tamijani, K. Sarabandi and G. M. Rebeiz, *IEEE Trans. Microwave Theory Tech.*, 2004, **52**, 1781–1789.

